International Journal of Nanoelectronics and Materials
IJNeaM
ISSN 1985-5761 | E-ISSN 2232-1535

Insights of MoO_3 HTL in Perovskite Solar Cells from a Simulation Perspective

Zulfanizam Abdul Wahab[a], Nabilah Ahmad Jalaludin[a], Mohd Khanapiah Nor[a], Ahmad Nizamuddin Muhammad Mustafa[a,b], Ahmad Syahiman Mohd Shah[c], Fauziyah Salehuddin[a] and Faiz Arith[a,*]

[a]*Faculty of Electronics and Computer Technology Engineering, Universiti Teknikal Malaysia Melaka, Hang Tuah Jaya,76100, Durian Tunggal, Malaysia*
[b]*Department of Materials, Faculty of Engineering, Imperial College London, London SW7 2AZ, UK*
[c]*Department of Electrical Engineering, College of Engineering, Universiti Malaysia Pahang, Lebuhraya Tun Razak, 26300 Gambang, Kuantan, Pahang, Malaysia*
**Corresponding author. faiz.arith@utem.edu.my*

ABSTRACT

The charge carrier conduction mechanism plays an important role in determining efficient Perovskite Solar Cells (PSCs), one of which lies in the Hole Transport Layer (HTL). Nowadays, the organic Spiro-Ometad HTL has been widely used in conventional PSCs, but the cell performance is still hindered and limited by the ambient humidity stability issue. Herein, a solid-state Molybdenum Trioxide (MoO_3) has been employed as the HTL in Pb-free PSCs. To comprehend its functional behaviour, a systematic study through the optimization of several critical parameters was carried out using SCAPs software. The high Power Conversion Efficiency (PCE) was achieved reaching 20.3% under AM 1.5 illumination, proving the high potential of MoO_3 as HTL in PSC. With optimized parameters, the distinctive solid-state MoO_3 has stood out among the top HTLs in PSC technology.

Keywords: *MoO_3, Perovskite Solar Cells, Hole Transport Layer, PCE*

1. INTRODUCTION

In today's world, environmental pollution has become a crisis that affects all nations, and there is an urgent need to find a solution. As a result, there is an increasing need for solar energy research. On the other hand, the lack of stability and endurance of perovskite solar cells is now an issue. The chemical deteriorates with time, resulting in a decrease in total efficiency [1]. To address this issue, further research must be carried out prior to commercialization. The results of this investigation will demonstrate how the solar cell might be improved. The optimisation of local current extraction is becoming an increasingly essential focus as the efficiency of industrial perovskite/silicon tandem solar cells approaches 30% [2].

Generally, perovskite solar cells consist of several key layers including the Hole Transport Layer (HTL), Electron Transport Layer (ETL) and perovskite absorber layer. Solid-state Molybdenum Trioxide (MoO_3) is considered a promising HTL in replacing conventional materials. In this project, SCAPs will be used to simulate perovskite-based solar cells in order to find the perfect parameters for producing high-efficiency perovskite solar cells. The goal of this research is to discover how to create high-efficiency perovskite solar cells. To get the most out of the solar cell, we are going to look into four different aspects: the cell's thickness, its doping concentration, its defect density, and its operating temperature. employing the Solar Cell Capacitance Simulator software, an investigation was conducted on the viability of employing molybdenum trioxide (MoO_3) as an alternative hole transport material for perovskite solar cells (SCAPS). Present, the most advanced and promising types of solar cells are flexible dye-sensitized and perovskite solar cells. These cells are particularly advantageous for mass production since they can be printed using a roll-to-roll method [3].The third generation of solar cells is a promising new technology that is just getting started. It is predicted that this technology will one day meet mankind's energy needs. This generation's purpose is to enhance cell efficiency while lowering costs, with the goal of adopting simple fabrication processes and keeping production costs low.

Photovoltaics (PV) is widely recognized as a prominent renewable energy source because to its exceptional effectiveness, efficiency, ecological compatibility, and affordability. In the year 2020, the production cost of photovoltaic (PV) energy has decreased to less than $0.05 per kilowatt-hour (kWh), aligning with the production prices of fossil fuels and coal, which stand at $0.05 and $0.03 per kWh, respectively. Through extensive research and advancements in photovoltaic (PV) technology, it is plausible to envision a future when solar energy becomes highly affordable and possesses the capacity to fulfil the energy needs of humanity [4]. The compound methylammonium lead iodide perovskite, often known as $CH_3NH_3PbI_3$ or $MAPbI_3$, is widely recognized as the pioneering example of a hybrid halide perovskite [5]. In general terms, a solar cell may be defined as a mechanism that generates electrical energy by directly converting sunlight through the photovoltaic phenomenon [6].
Among these options, spiro-OMeTAD remains the most widely utilized hole-transporting compound for achieving

high efficiency in perovskite solar cells (PSCs). Regrettably, the electrical conductivity of virgin spiro-OMeTAD is inadequate and often due to oxidation by atmospheric oxygen(O_2) [7]. The conventional hole transport layer (HTL), such as the doped 2,20,7,70-tetrakis(N,N-di-p-methoxy-phenylamine)-9,90-spirobi fluorene (spiro-OMeTAD), is well recognized to experience degradation due to moisture infiltration and elevated temperatures, despite its prevalent use in the fabrication of high-efficiency perovskite solar cells [8]. The transparent back electrode employed in this study was a dielectric/metal/dielectric (D/M/D) electrode.

Furthermore, the enhanced shelf stability and operational stability of PeLEDs based on MoO_3 can be related to the exceptional stability and neutral characteristics of MoO_3 films when compared to its equivalent, PEDOT:PSS [9]. Based on the data, it is clearly indicated that MoO_3 nanoparticles has therapeutic potential in the context of human breast cancer [10]. The results of device modelling indicate that the deposition of MoOx at room temperature exhibits favorable performance in both the normal and inverted architectures of the perovskite solar cell, achieving a promising efficiency of 18.25% [11]. Appropriate choices for transparent electrodes encompass thin metal films that are enclosed or layered with wide band gap dielectric materials, metallic nanowires, graphene, carbon nanotubes, transparent conductive oxides, and conducting polymers. [12].

In this paper, we investigated the influence of MoO_3 as an HTL material in the PSC on a variety of parameters. With an HTL layer thickness of 0.3 µm, cell efficiency reached 20.13%. This layer is thicker than the previous simulated report, which speeds up the manufacturing process and reduces the cost of cell manufacture. Thus, our findings indicate that PSC using MoO_3 as HTL has the potential to increase cell efficiency.

2. DEVICE SIMULATION

2.1 Poisson Equation:

$$\frac{d\,\varnothing(x)}{dx} = \frac{e}{\in \in}(\rho(x) - n(x) + N_D - N_A + \rho_p\ \rho_n \qquad [1]$$

$$g_D(E) = G_{Md}\exp[-(E - E_{pkd})\ /2\ _d \qquad [2]$$
$$g_A(E) = G_{Ma}\exp[-(E - E_{Pka})^2 / 2\ _a^2$$

Where$\boldsymbol{\phi}(x)$= Electrostatic Potential
$\in_0$= Vacuum Permittivity
$\in$r= Relative Permittivity
P and n = are hole and electron concentration
N_D=Charged impurities of donor
N_A= Charged impurities of acceptor
P_P and Pn are holes and electron distribution

SCAPS-1D was used to simulate PSC with MoO_3 as the HTL in this study. As illustrated in Figure 1, the PSC device structure consists of five major layers: FTO as the front contact, TiO_2 as the ETL, MAPbi3 as the absorber, MoO_3 as the HTL, and Au as the rear contact. Figure 2 depicts the band alignment of a simulation PSC device construction. A few factors were investigated to attain the best PSC cell efficiency based on the presence of MoO_3 as an HTL material. The layer thickness, MoO_3 doping density, device operating temperature, and interface defect on each layer were all altered and carefully analyzed.

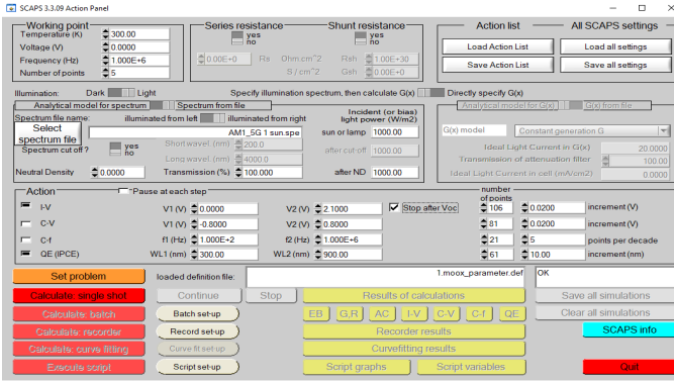

Figure 1. The SCAPs start-up panel or main panel.

In SCAPS-1D simulation, the sunlight is adjusted to the default illumination of AM1.5G. Table 1 shows the general SCAPS input and key parameters of each component. A few factors were investigated to acquire the best cell efficiency of the PSC based on MoO_3 as HTL materials. In this investigation, a solar cell capacitance simulator (SCAPS) is used to numerically predict the electronic properties of perovskite and crystalline silicon tandem solar cell devices [13].

The layer thickness, MoO_3 doping density, device operating temperature, and interface defect on each layer were all altered and carefully analyzed. In SCAPS-1D simulation, the sunlight is adjusted to the default illumination of AM1.5G, 100 MW.cm-2. Using 1D-SCAPS software and AM 1.5 illumination, critical parameters of the absorbent layer and HTL were optimized to produce the highest power conversion efficiency (PCE) [14].

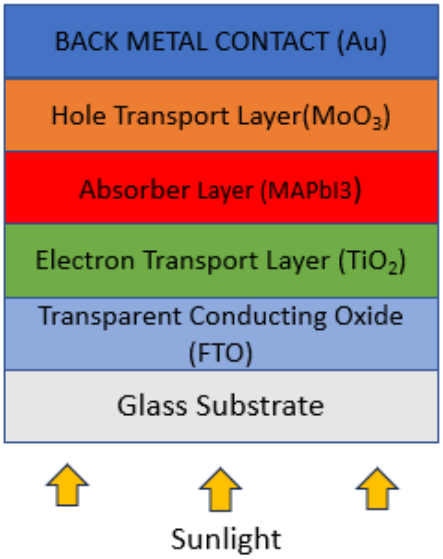

Figure 2. The simulated device structure of Perovskite Solar Cell.

Table 1 Parameters of the Material in device of Perovskite Solar Cell

Materials	MoO_3 [11]	Perovskite MAPbi3 [11]	TiO2	FTO
Thickness nm	250	330	50	370
Band gap (eV)	3.75	1.55	3.2	3.500
Electron affinity (eV)	2.20	3.90	3.90	4.00
Dielectric permittivity (relative)	4.45	6.50	9.00	9.00
CB effective density of states ($1/cm^3$)	1×10^{19}	1×10^{19}	1×10^{19}	1×10^{19}
VB effective density of states ($1/cm^3$)	1×10^{19}	1×10^{19}	1×10^{19}	1×10^{19}
Electron thermal velocity (cm/s)	1×10^{07}	1×10^{07}	1×10^{07}	1×10^{07}
Hole thermal velocity (cm/s)	1×10^{07}	1×10^{07}	1×10^{07}	1×10^{07}
Electron mobility (cm^2/Vs)	1.1×10^{03}	2×10^{0}	2×10^{16}	2×10^{1}
Hole mobility (cm^2/Vs)	1.1×10^{03}	2×10^{0}	1×10^{1}	1×10^{1}
Shallow uniform donor density ND ($1/cm^3$)	0×10^{0}	2×10^{13}	1×10^{16}	2×10^{19}
Shallow uniform acceptor density NA ($1/cm^3$)	2×10^{18}	0×10^{0}	0×10^{0}	0×10^{0}
Nt defect 1	1×10^{16}	2×10^{14}	1×10^{16}	1×10^{16}

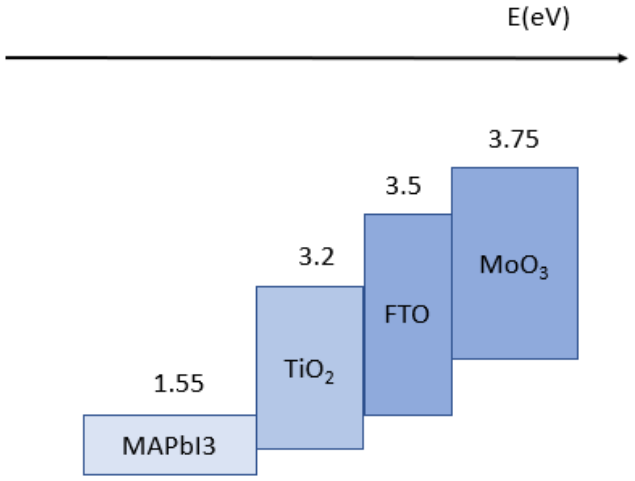

Figure 3. Energy level diagram of the PSC.

3. RESULT AND DISCUSSION

3.1. Analysis of MoO_3 Layer Thickness

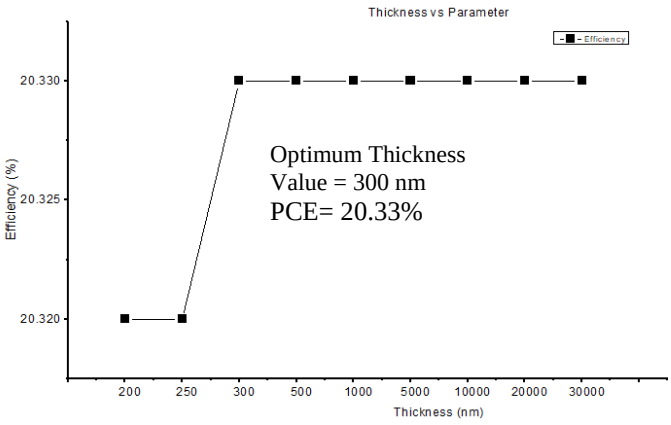

Figure 4. The optimum thickness of MoO_3 as HTL in the Perovskite Solar Cell.

The thickness of the HTL material is critical in the production of the PCE. Due to the greater travel distance of charges during the diffusion process, a thicker HTL layer may increase the likelihood of recombination. As a result of this circumstance, the device's efficiency suffers [7]. However, in this study, the efficiency of PSC based on molybdenum trioxide (MoO_3) increases with the layer thickness mainly due to the diffusion length factor. Then, eventually reaches a steady or saturated level at a thickness of 300 nm with an efficiency of up to 20.33% as shown in Figure 4. This is probably due to the strong charge carriers separation occur [15].

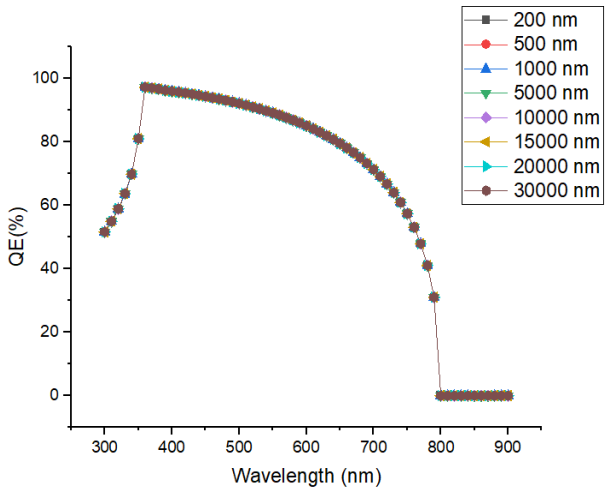

Figure 5. The Quantum Efficiency of MoO_3 as HTL in PSC.

In this phase of the simulation Figure 5, the quantum efficiency of the various MoO_3 thicknesses is evaluated and compared. During the duration of this simulation, the thickness is systematically altered within the range of 200 nm to 30,000 nm in order to examine the impact of the thickness parameter on the quantum efficiency. Based on the data presented in Figure 6, it can be observed that the quantum efficiency exhibits an upward trend as the wavelength rises, specifically at a wavelength of 300 nm. However, it is noteworthy that after the quantum efficiency reaches its maximum value of 100%, it subsequently decreases until it reaches a value of 0%. This phenomenon is observable through the examination of the Figure 5. No significant disparity in the quality of the quantum emitters (QEs) is seen across various thicknesses of the layers. Furthermore, the simulated spectra of the device were computed using SCAPS software, while also considering the experimental bandgaps of the active layer. Nevertheless, the optical phenomena, such as incomplete reflection, and the losses incurred due to recombination were not accounted for in this procedure [16].

3.2 Analysis of Working Temperature

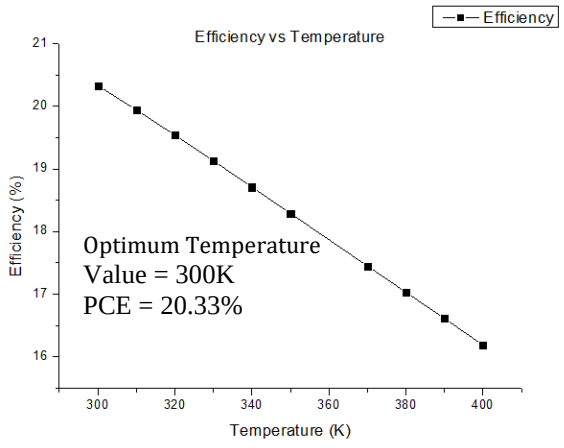

Figure 6. The Working temperature of the PSC.

Figure 6 shows the effect of temperature on cell performance, which provides an in-depth analysis for the purpose of applicability of solar cells in various location conditions. Here, the temperature was varied in a range from 280 K to 400 K. The impact of elevated temperatures on semiconductor devices is evident through the alteration and modulation of several parameters, including electron and hole mobility, carrier concentration, and material band gap. Consequently, there is a decrease in the rate of electron movement, thereby impacting the overall efficacy of the cell [17]. The bandgap of semiconductors decreases as temperature rises, causing the crystal lattice to expand and the interatomic connection to weaken. The velocity of charged particles increases as the temperature rises. The rate of electron and hole recombination, on the other hand, has increased. As a result, the quantity of available free carriers is reduced. When a result, as the operating temperature rises, the efficiency decreases [18]. As a result, because VOC is directly proportional to saturation, its value decreases as the temperature rises. The rate of electron and hole recombination increases with temperature, resulting in a drop in the number of electrons and free holes and reducing performance. According to the simulation, the best temperature is 300 K, which has a maximum efficiency of 20.33%.

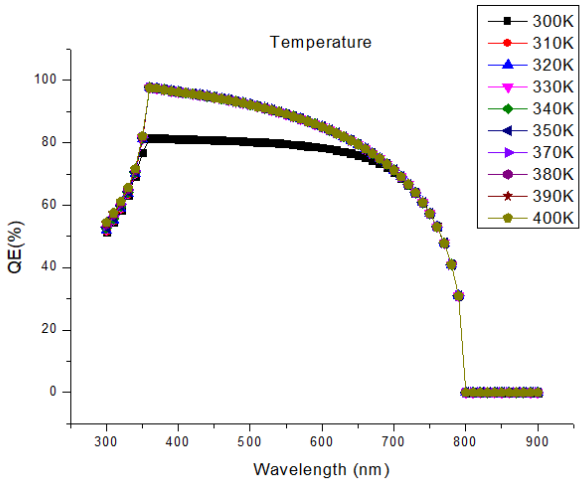

Figure 7. The Quantum Efficiency of the working temperature of the PSC.

The impact of temperature on the quantum efficiency of a system is seen in Figure 7. Figure 7 illustrates an increase in quantum efficiency from 50% to 100% when the wavelength transitions from 300 to 350 nm. When this phenomenon takes place, the graphical representation will exhibit a declining pattern within the wavelength range of 350 to 800 nm, accompanied by a reduction in quantum efficiency from 97.7% to 0%. The system will not attain a condition of saturation until the wavelength reaches a value of 900 nm. In contrast, at a temperature of 300 K, Figure 6 illustrates that the highest point is comparatively lower than the other data points, representing around 80% of the temperature magnitude observed in the rest of the data. The decrease in bandgap within the solar cell

resulting from an increase in temperature is known to exert an impact on the quantum efficiency.

3.3 The Analysis of Doping Concentration, N_A

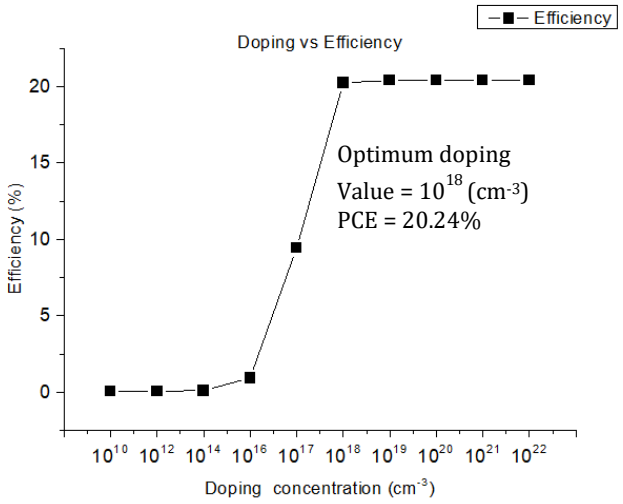

Figure 8. The graph of doping concentration of the MoO_3 as HTL in PSC.

This phenomenon arises due to the direct correlation between the efficiency of solar cells and the density of doping acceptors. The increase in temperature leads to a decrease in the surface and layer resistance of the heterojunction tunnelling layer (HTL), hence facilitating an augmentation in the current flow within the cell. In contrast, doping concentrations progressively increase to a level that elicits the Moss-Burstein effect due to the substantial extent of doping activity. The formation of an extra recombination centre would ultimately lead to a degradation in the performance of solar cells.

Doping levels ranging from 10^{10} cm^{-3} to 10^{22} cm^{-3} are depicted in Figure 8, which presents the results of a simulation examining the link between Efficiency and Doping Concentration. Because of this, the data may have its optimisation improved. According to the Figure 8, when the amount of doping reaches 10^{20}, the efficiency will reach its maximum level and become saturated. This is a result of the fact that the efficiency of solar cells rises in direct proportion to the quantity of doping acceptors present. As a consequence of this increase, the surface and layer resistance of the hole transport layer (HTL) will decrease, which will make it possible for the cell's current flow to grow. A decrease in the quality of the doping levels and the doping process in the absorber layer is the primary factor that contributes to the production of defects and the performance of the device [7]. Doping concentrations, on the other hand, continue to rise to the point where they activate the Moss-Burstein effect due to the volume of doping. The additional recombination centre that will be formed as a result of this will eventually degrade the performance of solar cells [19]. The constant doping concentration is set at 10^{18}, the value at which the efficiency is 20.24% and the concentration stabilizes.

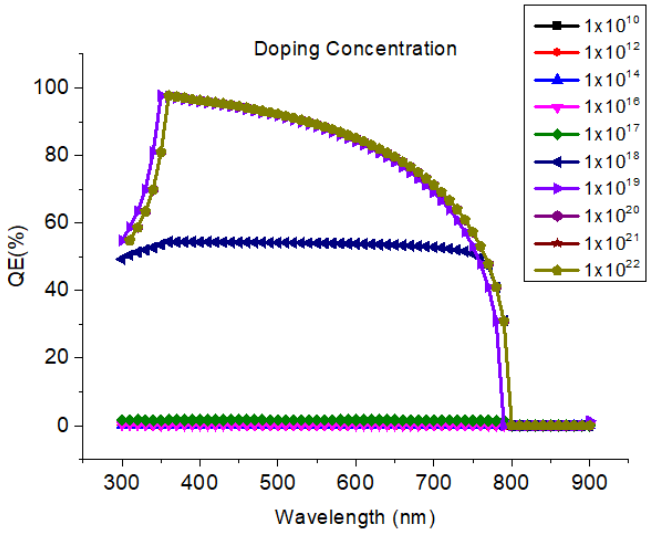

Figure 9. The quantum efficiency of the doping concentration of the PSC.

The impact of doping concentration on quantum efficiency is shown graphically in the following Figure 9. Figure 9 illustrates how the amount of doping in a material might affect its quantum efficiency. Figure 9indicates that as the amount of doping grows, so does the quantum efficiency; however, at certain doping concentrations, quantum efficiency reduces; for example, at 1×10^{18}, the value of quantum efficiency lowers to 50. This is a result of the fact that the efficiency of solar cells rises in direct proportion to the quantity of doping acceptors present. As a consequence of this rise, the surface and layer resistance of HTL reduces, which paves the way for an increase in the cell's current flow. In spite of this, doping concentrations continue to rise as a direct consequence of excessive doping, to the point where the Moss-Burstein effect comes into play. Because of the greater recombination centre that is created, the performance of solar cells will gradually deteriorate [19].

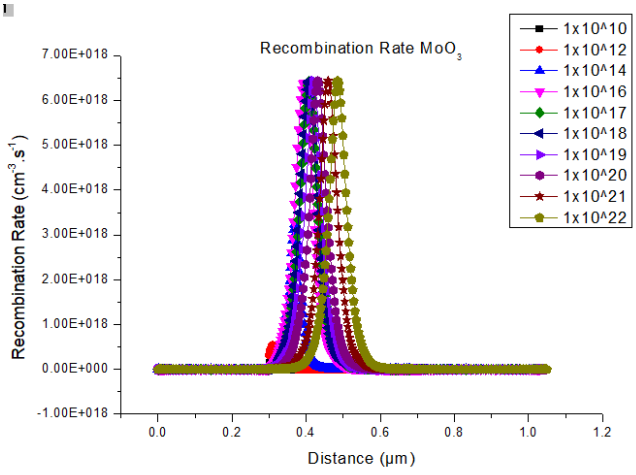

Figure 10. The Recombination Rate of PSC with MoO_3 as HTL.

From Figure 10, it was found that the rate of recombination in MoO_3 as HTL in PSC reached its highest point between the doping 1×10^{10} cm^{-3} until 1×10^{22} cm^{-3}. According to the findings presented in Figure 10, the bulk of recombination took place at a spacing ranging from 0.3 to 0.6 micrometres regardless of the doping density. As the recombination centres form, a number of the photo-generated carriers are prevented from reaching the solar cell terminal and are instead collected. As a direct consequence of this, the lifetime of free carriers is shortened, which disrupts the flow of current.

3.4 Analysis of Defect Density of MoO_3

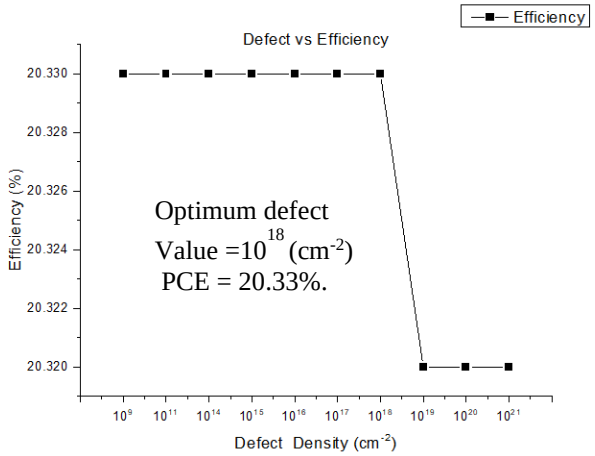

Figure 11. The Defect density of the PSC with MoO_3 as HTL.

The reason for this phenomenon is that an escalation in the defect results in an amplified recombination rate on films of inferior quality. Consequently, this leads to a diminished charge carrier dispersion length and a reduced carrier lifespan. The rationale behind this phenomenon is attributed to the positive correlation between defect augmentation and recombination rate elevation. Furthermore, a positive association exists between the increase in defect density and the corresponding increase in recombination centre density, resulting in a decrease in the overall efficiency of the cell.

Figure 11 shows the simulation investigates the relationship between efficacy and defect density. As a subsequent stage, the fault density is modified between10^9 (cm^{-2}) to 10^{21} (cm^{-2}). In order to optimise this parameter, we account for this range. According to the Figure 11, as the defect increases, the efficacy will level off or become saturated between 10^9 (cm^{-2}) to 10^{18} (cm^{-2}). At defect 10^{19} (cm^{-2}) and above, efficiency will begin to decrease. On low-quality films, however, an increase in the defect density leads to an increase in the recombination rate, which in turn decreases the charge carrier dispersion length and the carrier lifetime. The decrease in short circuit current indicates that the reverse saturation current of the proposed tandem inorganic solar cell is increasing[20] In addition, there is a correlation between the defect density and the recombination rate density, which leads to a decrease in the cell's efficacy. At an efficacy level of 20.33% percent, the defect density has a constant thickness of 10^{18} (cm^{-2}).

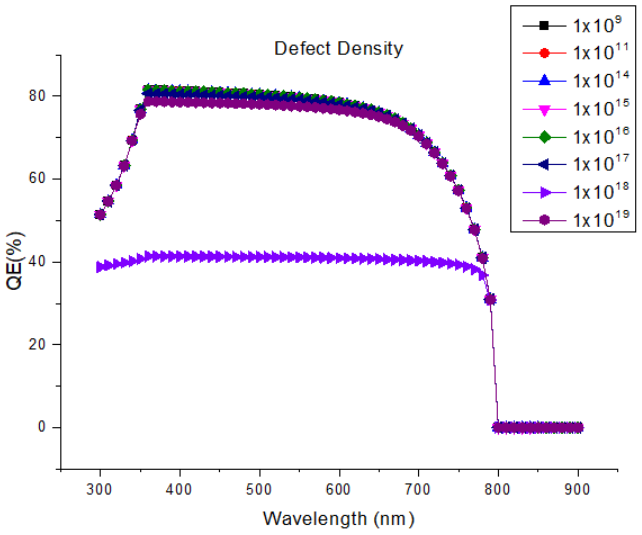

Figure 12. The Quantum efficiency defect of the PSC with MoO_3 as HTL.

Figure 12 depicts the effect of defect concentration of quantum efficiency vs. wavelength. The dark current is held at zero current from negative voltage to 1.1 V in the normal situation, suggesting that there is no leakage current in the reverse bias. The Figure 12 first shows an increase in quantum efficiency from 50 to 80%; however, the value then continues to drop until it hits 0 at a wavelength of 800 nm. When there is a defect of 1x10-18, however, the quantum efficiency remains constant at 41% until it reaches a wavelength of 800 nm, at which time it decreases to 0%. This occurs when the quality of the layers deteriorates, resulting in an increase in the rate of recombination and, as a result, an increase in the number of traps at the interface.

3.5 The Analysis of Dark and Light Illumination

In Figure 13 the dark current is held at zero current from negative voltage to 1.1 V in the normal situation, suggesting that there is no leakage current in the reverse bias.

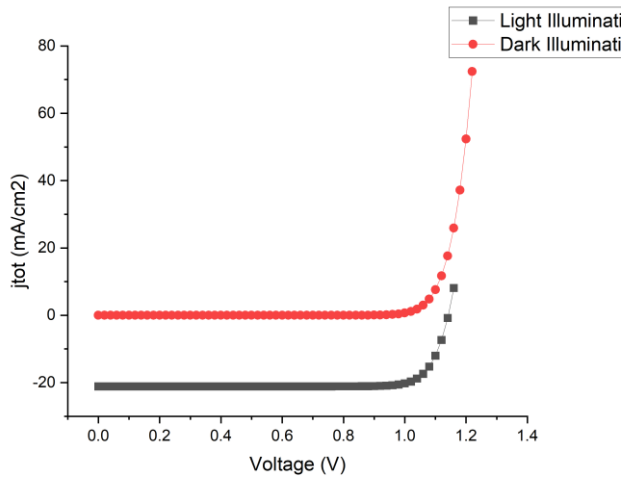

Figure 13. The Dark and Light of PSC with MoO_3 as HTL.

Both materials illustrate that the dark and light currents do not overlap, which is a positive thing. Because solar cells may function successfully in both low and bright lighting circumstances, the solar cell in this study is examined in both of these lighting conditions. Furthermore, the recombination rate occurs at an absorbent layer of $1\times10^{18}cm^{-3}$. Figure 13 depicts black illumination that occurs at zero current and increases to 1.1 V. This implies that there is no leakage current in the reverse bias, implying that the simulation can run without error. Furthermore, Figure 14 shows that there is no overlap between the distinct layers, indicating efficient current conducting.

Table 2 The Optimise Result of the Perovskite Solar Cell

Parameter	MoO_3 [This work]	MoO_3 [11]
Thickness (nm)	300	50-250
Temperature (K)	300	300
Doping donor density N_D (cm^{-3})	10^{18}	10^{18}
Defect density (cm^{-2})	10^{17}	10^{15}
V_{OC} (V)	1.217	0.95
Jsc(mA/cm^2)	21.119	22.58
FF(%)	84.99	82.56
PCE (%)	20.13	17.82
Thickness (nm)	300	50-250

Previous study [11] has determined that the molybdenum trioxide (MoO_3) has a fill factor of 82.56%, a V_{OC} (V) of 0.95 volts, and a J_{SC} of 22.58 milliamperes per square centimetre. The PCE value is 17.82%. After completion of all four parameters optimization, the best output obtained for Voc (V) was 1.217, J_{SC} was 21.119 (mA/cm2), the FF was 84.99%, and the PCE was 20.3%. Those cell performance were obtained with the MoO_3 layer thickness of 300 nm, at working temperature of 300 K, doping density at 1×10^{18} (cm^{-3}) and with tolerable the defect density of 1×10^{-17} (cm^{-2}). Ultimately, with regard to the performance capability enhancement (PCE), the optimised result of 20.3% displays an increase of 11.48% in comparison to the previous report of 17.82%, with a similar MoO_3 ETL structure.

4. CONCLUSION

The ideal key parameters for PSC using MoO_3 as HTL have been determined. The value of PCE has demonstrated that cell efficiency has been increased by in-depth investigation. The performance of the device is improved by optimizing the key parameter of MoO_3 in PSC. Overall, by using optimized parameters and regulating the defect density to a particular degree, the cell efficiency of the simulated PSC has effectively boosted. All four main parameter including the layer thickness, doping concentration, working temperature as well as the defect density has shown an influence in determining the solar cell performance. The study successfully demonstrated the considerable potential of MoO_3 as a hole transport layer (HTL) in perovskite solar cells (PSC), achieving a notable power conversion efficiency (PCE) of 20.3% under AM 1.5 illumination. The solid-state MoO_3, when its parameters are optimized, has demonstrated exceptional performance as a hole transport layer (HTL) in perovskite solar cell (PSC) technology. This work therefore gives a clear understanding that may be used as parameter guidance in the fabrication of the PSC.

ACKNOWLEDGMENTS

This work was supported by Universiti Teknikal Malaysia Melaka and Ministry of Education Malaysia under Grant PJP/2022/FKEKK/S01865.

REFERENCES

[1] S. Sharma, K. K. Jain, and A. Sharma, "Solar Cells: In Research and Applications—A Review," *Mater. Sci. Appl.*, vol. 06, no. 12, pp. 1145–1155, 2015, doi: 10.4236/msa.2015.612113.

[2] M. Padilla, B. Michl, B. Thaidigsmann, W. Warta, and M. C. Schubert, "Short-circuit current density mapping for solar cells," *Sol. Energy Mater. Sol. Cells*, vol. 120, no. PART A, pp. 282–288, 2014, doi: 10.1016/j.solmat.2013.09.019.

[3] N. S. Noorasid *et al.*, "Low-temperature sol-gel synthesized TiO2 with different titanium tetraisopropoxide (TTIP) molarity for flexible emerging solar cell," *J. Sol-Gel Sci. Technol.*, vol. 109, no. 3, pp. 826–834, 2024, doi: 10.1007/s10971-024-06310-2.

[4] N. S. Noorasid *et al.*, "Current advancement of flexible dye sensitized solar cell: A review," *Optik (Stuttg).*, vol. 254, no. May 2021, p. 168089, 2022, doi: 10.1016/j.ijleo.2021.168089.

[5] C. Bhoomanee, P. Ruankhama, S. Choopun, A. Prathan, and D. Wongratanaphisan, "Effect of Al-doped zno for electron transporting layer in planar perovskite solar cells," *Mater. Today Proc.*, vol. 17, pp. 1259–1267, 2019, doi: 10.1016/j.matpr.2019.06.014.

[6] N. S. Noorasid, F. Arith, A. Y. Firhat, A. N. Mustafa, and A. S. M. Shah, "SCAPS Numerical Analysis of Solid-State Dye-Sensitized Solar Cell Utilizing Copper (I) Iodide as Hole Transport Layer," *Eng. J.*, vol. 26, no. 2, pp. 1–10, 2022, doi: 10.4186/ej.2022.26.2.1.

[7] U. Mandadapu, S. V. Vedanayakam, and K. Thyagarajan, "Simulation and Analysis of Lead based Perovskite Solar Cell using SCAPS-1D," *Indian J. Sci. Technol.*, vol. 10, no. 11, pp. 1–8, 2017, doi: 10.17485/ijst/2017/v10i11/110721.

[8] X. Zheng *et al.*, "Organic-inorganic hybrid hole transport layers with SnS doping boost the performance of perovskite solar cells," *J. Energy Chem.*, vol. 68, pp. 637–645, 2022, doi: 10.1016/j.jechem.2021.11.034.

[9] D. Liang, X. Xue, J. Peng, and W. Ji, "Perovskite light-emitting diodes with solution-processed MoO3 films as the hole-transport layers," *J. Lumin.*, vol. 256, no. December 2022, p. 119621, 2023, doi: 10.1016/j.jlumin.2022.119621.

[10] J. Kumari and P. Mangala, "Fabrication and Characterization of Molybdenum Trioxide Nanoparticles and their Anticancer, Antibacterial and Antifungal Activities," *Malaysian J. Chem.*, vol. 24, no. 1, pp. 36–53, 2022, doi: 10.55373/mjchem.v24i1.1265.

[11] F. Ali *et al.*, "Prospects of e-beam evaporated molybdenum oxide as a hole transport layer for perovskite solar cells," *J. Appl. Phys.*, vol. 122, no. 12, 2017, doi: 10.1063/1.4996784.

[12] M. B. Upama *et al.*, "Low-temperature processed efficient and colourful semitransparent perovskite solar cells for building integration and tandem applications," *Org. Electron.*, vol. 65, no. November 2018, pp. 401–411, 2019, doi: 10.1016/j.orgel.2018.11.037.

[13] S. Sarker *et al.*, "A SCAPS simulation investigation of non-toxic MAGeI3-on-Si tandem solar device utilizing monolithically integrated (2-T) and mechanically stacked (4-T) configurations," *Sol. Energy*, vol. 225, no. July, pp. 471–485, 2021, doi: 10.1016/j.solener.2021.07.057.

[14] N. S. N. M. Alias, F. Arith, A. N. M. Mustafa, M. M. Ismail, S. A. M. Chachuli, and A. S. M. Shah, "Compatibility of Al-doped ZnO electron transport layer with various HTLs and absorbers in perovskite solar cells," *Appl. Opt.*, vol. 61, no. 15, pp. 4535–4542, May 2022, doi: 10.1364/AO.455550.

[15] H. Abdulsalam, G. Babaji, and H. T. Abba, "The Effect of Temperature and Active layer thickness on the Performance of CH3NH3PbI3 Perovskite Solar Cell: A Numerical Simulation Approach.," *J. Found. Appl. Phys.*, vol. 5, no. 2, pp. 141–151, 2018.

[16] S. Karthick, S. Velumani, and J. Bouclé, "Experimental and SCAPS simulated formamidinium perovskite solar cells: A comparison of device performance," *Sol. Energy*, vol. 205, no. March, pp. 349–357, 2020, doi: 10.1016/j.solener.2020.05.041.

[17] N. S. N. M. Alias, F. Arith, A. N. Mustafa, M. M. Ismail, N. F. Azmi, and M. S. Saidon, "Impact of Al on ZnO Electron Transport Layer in Perovskite Solar Cells," *J. Eng. Technol. Sci.*, vol. 54, no. 4, 2022, doi: 10.5614/j.eng.technol.sci.2022.54.4.9.

[18] A. Kuddus, M. F. Rahman, S. Ahmmed, J. Hossain, and A. B. M. Ismail, "Role of facile synthesized V2O5 as hole transport layer for CdS/CdTe heterojunction solar cell: Validation of simulation using experimental data," *Superlattices Microstruct.*, vol. 132, no. June, 2019, doi: 10.1016/j.spmi.2019.106168.

[19] P. Chelvanathan *et al.*, "Effects of RF magnetron sputtering deposition process parameters on the properties of molybdenum thin films," *Thin Solid Films*, vol. 638, pp. 213–219, 2017, doi: 10.1016/j.tsf.2017.07.057.

[20] A. Kuddus, M. F. Rahman, J. Hossain, and A. B. M. Ismail, "Enhancement of the performance of CdS/CdTe heterojunction solar cell using TiO2/ZnO bi-layer ARC and V2O5BSF layers: A simulation approach," *EPJ Appl. Phys.*, vol. 92, no. 2, pp. 1–14, 2020, doi: 10.1051/epjap/2020200213.